Diagnosing systematic differences in predicted wind turbine array-array interactions

Pryor, S.C.; Shepherd, T.J.; Volker, P.J.H.; Hahmann, A.N.; Barthelmie, R.J.

Published in:
Journal of Physics: Conference Series

Link to article, DOI:
10.1088/1742-6596/1618/6/062023

Publication date:
2020

Document Version
Publisher's PDF, also known as Version of record

Diagnosing systematic differences in predicted wind turbine array-array interactions

Diagnosing systematic differences in predicted wind turbine array-array interactions

S.C. Pryor[1], T.J. Shepherd[1], P.J.H. Volker[2], A.N. Hahmann[2], R.J. Barthelmie[3]

[1]Department of Earth & Atmospheric Sciences, Cornell University, Ithaca, NY14853, USA
[2]Department of Wind Energy, Technical University of Denmark, DK4000 Roskilde, Denmark
[3]Sibley School of Mechanical & Aerospace Engineering, Cornell University, Ithaca, NY14853, USA
sp2279@cornell.edu

Abstract. Improved quantification of the spatial extent and intensity of wind farm wakes is urgently needed given the rapid pace of expansion of installed capacity both on- and off-shore. We present and analyse long-term, high-resolution simulations of whole wind farm wakes conducted for real-world wind turbine installations performed with the two wind farm parameterizations (EWP and Fitch) designed for use with the Weather Research and Forecasting model. We document differences in the formulation of these two parameterizations and demonstrate their impact on simulated wind farm wakes. Divergence between the schemes in terms of wake spatial extent and magnitude is maximized under low/moderate turbulent kinetic energy (TKE < 0.3 m^2s^{-2}) and wind speeds between cut-in and rated ($U \approx$ 4-12 ms^{-1}). Thus, it is under those conditions that model predictions of the intensity/spatial extent of wind farm wakes are inferred to have highest uncertainty. A framework is introduced based on these simulations that can be used to aid planning for experiments such as AWAKEN. It could be used to identify where and when observational data would be most beneficial in differentiating relative skill of the two parameterizations and identifying areas where modifications to the schemes are necessary to improve fidelity.
Keywords: Wind farm wakes. Numerical simulations. Mesoscale. Intra-farm effects.

1. Introduction

Total wind turbine installed capacity (IC) in the United States of America (USA) is approximately 106 GW (end of 2019) and projections indicate over 44 GW of additional IC either under construction or in advanced development, including over 7 GW of offshore wind [1]. Much of the new development is focussed onshore in areas with substantial existing wind turbine installations [1]. Total European wind turbine IC is approximately 189 GW (as of end of 2018, [2]), with additions of 90 GW projected over the next five years [3]. The majority of this growth is anticipated to be onshore in Germany, Spain and the UK which already have high IC [2]. Offshore expansion is projected to be principally focused on the North Sea which had an installed capacity of 13 GW at the end of 2018 [2]. Thus, projected increases in IC both in Europe and the USA are concentrated on areas with substantial existing installed capacity densities (ICD), which implies increasing potential for wind farm-farm interactions.

In the third quarter of 2019, Denmark's Ørsted issued a statement alongside its Q3 results explaining that it was downgrading anticipated internal rate of return for several offshore wind projects in Europe and Taiwan, from 7.5 to 8.5% down to 7 to 8%. One cause identified by Ørsted was; 'the wake within wind farms and between neighbouring wind farms. There is a wake after each wind turbine where the wind slows down. As the wind flow continues, the wake spreads and the wind speed recovers. This effect, with wind turbines shielding and impacting each other, has been subject to extensive modelling

by the industry for many years, and it is still a highly complex dynamic to model. Our results point to a higher negative effect on production than earlier models have predicted' (https://www.greentechmedia.com/articles/read/orsted-warns-industry-not-to-ignore-forecast-downgrades). This effect is not specific to Ørsted and affects the entire industry.

For the reasons described above, there is increasing interest in high-fidelity simulations of whole wind farm wakes and farm-farm interactions in support of more accurate energy yield projections for new developments. Evaluating existing models and developing improved models of the atmospheric physics of large wind farm wakes are the goals of our research.

Research presented herein uses the Weather Research and Forecasting (WRF, v3.8.1) model to simulate and quantify whole wind farm wakes. Two wind farm parameterizations are available for use in WRF: Fitch [4] and the Explicit Wake Parameterization (EWP) [5]. These parameterizations do not seek to describe the wakes from individual wind turbines but rather the cumulative wake derived from all wind turbines in grid cells that have typical dimensions of 1–5 km by 1–5 km (see guidance in ref [6]). They are thus designed to capture the integrated wake from multiple wind turbines (i.e. whole wind farm wakes). The wind farm parameterizations differ in multiple ways [7, 8] but most important is the manner in which they seek to parameterize expansion, and hence recovery, of the wake. In Fitch turbulent kinetic energy (TKE) is added in grid cells across the swept rotor plane(s) by wind turbine(s) in a given grid cell in an amount proportional to the difference between the thrust and power coefficients at that wind speed for that/those wind turbine(s) [4]. In most situations this added TKE exceeds the ambient TKE in grid cells in which wind turbine(s) are located [4]. The added TKE is designed to be advected with the prevailing flow into adjacent grid cells and acts to enhance mixing in these downstream grid cells leading to expansion and recovery of the wake. In EWP the increase in grid-cell average turbulence due to the action of the wind turbine rotor(s) is parameterized using a wake expansion length scale which is a function of the turbulent diffusion coefficient from the planetary boundary layer scheme, hub-height wind speed and a rotor length scale [5]. This approach means the wake is expanded within the grid cell(s) in which wind turbine(s) are located. The modified wake is advected downstream and further eroded by mixing in of higher momentum air down the velocity gradient. A second point of difference between the two schemes is that the wake centre is displaced upward from the wind turbine hub-height in the Fitch scheme but not in EWP [5].

Previous studies have shown simulations with these two wind farm parameterizations exhibit substantial differences in terms of the:

(i) Area over which wind farm wakes are manifest and thus the probability of farm-farm interactions [5, 7].
(ii) Intensity of wind farm wake velocity deficits and thus magnitude of farm-farm interactions [7, 9].
(iii) Seasonality and diurnal variability of (i) and (ii).
(iv) Influence of wind turbine arrays on near-surface climate variables [8, 9].

Past research has also indicated that the magnitude and sign of the differences between the two parameterizations varies according to location. For example, monthly gross simulated power production for wind turbines in the US state of Iowa is 4.6–5.6% higher when EWP is applied than Fitch [7], consistent with evidence of shorter recovery distances for wakes using EWP [9]. However, simulations of the Horns Rev offshore wind farm for a freestream wind speed of 10 ms^{-1}, near-neutral stability and a surface roughness length of 0.2 mm (thus low freestream TKE) found the downstream recovery distance (to <5% velocity deficit) was considerably shorter (11 km v 21 km) in simulations with Fitch [5]. The inference is that the ambient atmospheric conditions (e.g. atmospheric stability and TKE), and potentially wind turbine ICD play key roles in both dictating relative wake intensity and downstream persistence from the two wind farm parameterizations and in explaining the divergence between them. Under the assumption that divergence of wind farm wake characteristics (extent and intensity) from the two schemes can be viewed as a metric of the uncertainty in wind farm wake simulation, quantifying the magnitude and root causes of the divergence will aid in improving the parameterizations to make better preconstruction projections of expected annual energy production (AEP) and reducing the uncertainty on AEP for wind turbine arrays deployed in the wind shadow of existing arrays.

2. Objectives

We analyse long-term high-resolution simulations conducted over the US Midwest with the WRF model using both the Fitch and EWP wind farm parameterizations to:

(i) Improve fundamental understanding of parameterization behaviour under real world conditions.
(ii) Identify under what conditions wakes from the parameterizations exhibit greatest differences.
(iii) Provide a framework for use in designing a field experiment to differentiate the fidelity of, and differential credibility of, the two wind farm parameterizations. Such a field experiment is currently in the planning phase within the US. The proposed American Wake Experiment (AWAKEN) is designed to provide uniquely detailed observations of wind turbine wake interactions and aerodynamics, advance understanding of wake behaviour and validate wake models across a range of scales and complexity (see details at: https://openei.org/wiki/AWAKEN).

Virtually all of the 105 GW of the wind turbine (WT) IC in the US is onshore [1]. Thus, AWAKEN and the analyses presented here focus on onshore conditions. However, this work is intended to improve model formulations and hence should also benefit the offshore industry.

3. Methodology

We conducted long-term simulations (December 2007 to August 2008, inclusive) with WRF (v3.8.1) using all 3100 WT installed in Iowa as of the end of 2014 (WT characteristics such as hub-height, rotor diameter, power and thrust coefficients are specified for each individual WT as in ref [10, 11]). The outer domain (d01) is resolved using a grid spacing of 12 km × 12 km and covers an area extending from ~103 to 83°W and ~33.5 to 49.5°N (Figure 1(a)). There are three inner domains where-in WRF is applied at convection-permitting resolutions of 4 km × 4 km with 57 vertical layers (Figure 1(b)). In the first inner domain no wind turbines are included (d02_noWT), in the second the Fitch scheme is applied (d02_Fitch), and in the third EWP is employed (d02_EWP). Key simulation settings include use of the Mellor-Yamada-Nakanishi-Niino 2.5 PBL scheme (because this is the only PBL scheme Fitch is designed to operate within) and advection of TKE. Further details of the simulation are given in ref [7].

Here we focus on results for a portion of the inner domain centred on the Pomeroy wind farm cluster (Figure 1(b), and in detailed in Figure 2). This sub-domain comprises 20, 4 km by 4 km grid cells in longitude (west-east) and 27, 4 km by 4 km grid cells in latitude (south-north). It contains three distinct wind farm developments. The central one is referred to herein as Pomeroy and is an agglomeration of five developments. It has a total of 213 wind turbines (models; GE1.5-77, SWT-2.3-101 and G90-2.0) with hub-heights ranging from 80 to 100 m, rotor diameters (D) of 77 to 101 m and rated capacities of 1.5 to 2.3 MW (see details in ref [8]). There are also wind turbine clusters to the west (west of 95.2º W, and thus located outside of the sub-domain), and southwest and southeast of Pomeroy (Figure 2). Results from the Pomeroy wind farm cluster are used to identify where in space and time the schemes exhibit largest systematic differences and also to illustrate how such simulations might be used to help design a parameterization verification and validation experiment such as AWAKEN. Output from the sixth model layer for a grid cell in the centre of the Pomeroy sub-domain for no-WT domain (d02_noWT) is used to describe freestream TKE and wind speed (U) conditions. WRF employs a hydrostatic-pressure vertical coordinate system so vertical levels are not at a fixed height above local ground level either in space or time. The sixth model level equates to heights of 72 to 93 m in the centre of the Pomeroy domain, with a mean value of 82 m. TKE values reported from this model level derive directly from the Mellor-Yamada-Nakanishi-Niino 2.5 PBL scheme, without added TKE from the wind farms. The areal extent and intensity of the wind farm wake is defined in each 10-minute period using the fractional velocity deficit ($vd_{(x,y,z,t)}$) near WT hub-height (at $z = 6$); Fitch (or EWP) minus no-WT in each grid cell:

$$vd_{(x,y,z,t)} = \left(\frac{U_{d02\_XXXX(x,y,z,t)} - U_{d02\_noWT(x,y,z,t)}}{U_{d02\_noWT(x,y,z,t)}}\right) \quad (1)$$

Where; U_{d02_XXXX} = wind speed output in a given grid cell (x,y), vertical level ($z = 6$) and time step (t). *XXXX* is Fitch or EWP, and U_{d02_noWT} indicates output from the noWT inner domain. Two descriptive metrics are defined based on $vd_{(x,y,z,t)}$:

(i) Areal extent of the wake is the fraction of grid cells in the Pomeroy sub-domain (i.e. $x = 1{:}20$, $y =$

1:27) close to WT hub-height (z = 6) with $vd_{(x,y,z,t)} \geq 5\%$ in each 10-minute period in a specified calendar month. While the simulated power production from an individual wind turbine is dictated principally by the freestream wind speed, it is the joint probability of wind speeds (U) and TKE (plus wind direction) that dictate wind farm wake behaviour and the probability that wakes from upstream wind turbine arrays will impinge upon downstream WT power plants. Thus, wake areal extent is described below as a function of the co-occurrence of U and TKE in given classes. In this analysis results of the areal extent of wakes in each 10-minute period are conditionally sampled by the prevailing freestream (d02_noWT) U and TKE to examine the atmospheric conditions under which wake extents are maximized and also when the output from the two schemes exhibit largest differences. An average areal extent of the wake of 20% in a class of joint occurrence of freestream hub-height U = X and TKE = Y, indicates one-fifth or 108 of the 540 grid cells had a mean fractional $v_d \geq 5\%$ when the freestream U = X and TKE = Y. Values are only shown for TKE = 0 to 1 m^2s^{-2}, and in TKE|U cells with more than ten members.

(ii) Mean fractional velocity deficit in each grid cell ($<vd_{(x,y,z=6,t=1:n)}>$) and mean added TKE close to WT hub-height (z = 6) computed over a time interval (t = 1:n) is depicted spatially by calendar month. Further the spatial extent of the wakes is expressed using two thresholds of $<vd_{(x,y)}>$ (5% and 2%). This analysis thus shows the mean extent of waked areas averaged over all ten-minute periods and hence the average wind farm extent integrated over all freestream U and TKE in that month.

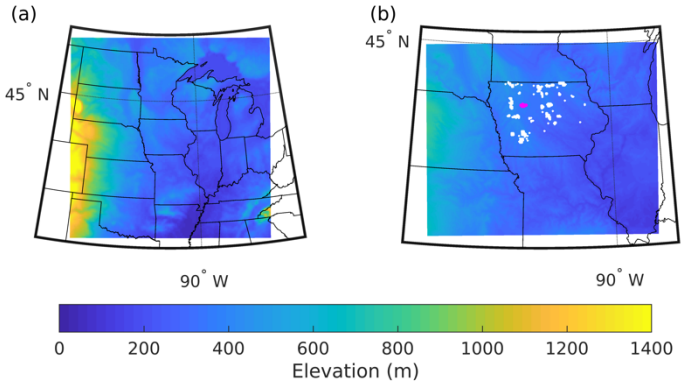

Figure 1. Map of the terrain in the (a) outer domain (grid resolution 12 km), (b) inner domain (grid resolution 4 km). Also shown are the location of 4 km by 4 km grid cells in which one of more wind turbine(s) is located (white) and the Pomeroy wind cluster (magenta).

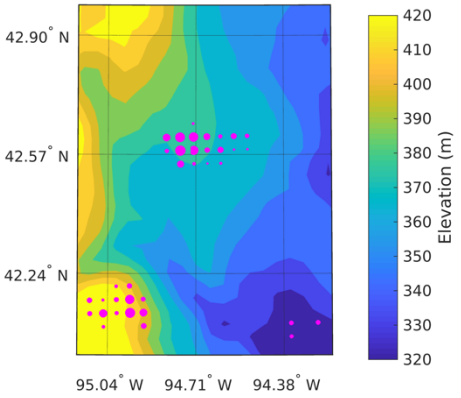

Figure 2. Terrain elevation in the sub-domain around the Pomeroy wind cluster of 20 (west-east) by 27 (south-north) grid cells. The magenta symbol diameter scales with WT installed capacity in each 4 km grid cell.

TKE is used here as a primary measure of the freestream (ambient) turbulence intensity and thus the propensity of the atmosphere to exhibit mixing and thus dissipation of wakes. TKE is strongly related to measures of the dynamic stability such as the gradient Richardson number [12] computed from:

$$Ri = \left(\frac{g}{T_v}\frac{\Delta\theta}{\Delta z}\right)/\left(\frac{\Delta U}{\Delta z}\right)^2 \qquad (2)$$

Where θ is potential temperature, g is gravity, T_v is virtual temperature, U is wind speed and z is height. Large magnitude negative gradient Richardson numbers indicate strong buoyancy-induced instability (unstable conditions) and high TKE, Ri values close to zero are indicative of near-neutral stability, dominance of mechanical forcing of turbulence and moderate TKE, and large positive Ri values are indicative of stably stratified flow and low TKE (Figure 3).

4. Results

4.1 Flow climate

The frequency of power producing wind speeds is generally highest in the spring months, with over

80% of 10-minute periods having a freestream wind speed (U) in the 6th model layer in the Pomeroy sub-domain in excess of 5 ms^{-1}, while only 70% of periods exhibit $U > 5$ ms^{-1} in the summer months (Figure 4). Overall, 80% of 10-minute periods exhibit freestream TKE < 1 m^{2}s^{-2}, and 40% exhibit freestream TKE < 0.2 ms^{-1} (Figure 5). TKE is generally low during winter and there is a marked transition in April to an increased frequency of high TKE values which is sustained through the summer (Figure 5). Median TKE in the centre of the Pomeroy sub-domain is < 0.25 m^{2}s^{-2} in December and January, is 1 m^{2}s^{-2} during April, and remains above 0.45 m^{2}s^{-2} during summer (Figure 5).

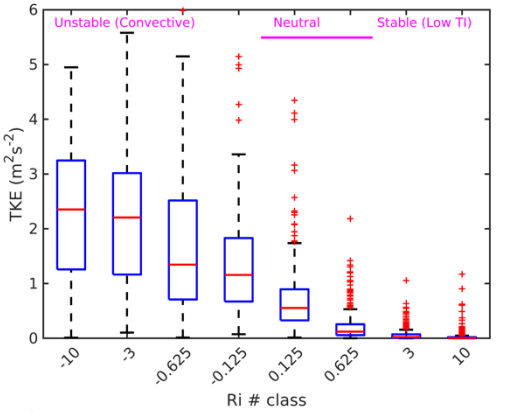

Figure 3. Box plot of freestream TKE (at z = 6) sampled by freestream gradient Richardson number (computed for the layer extending across the rotor plane, z = 3 to z = 9) in the centre of the Pomeroy sub-domain. In each the box the central (red) bar denotes the median. The box extends from the 25th to 75th percentiles. The whiskers extend to the most extreme points that are not considered outliers and the outliers are noted by the red plus symbols. An outlier is defined as any value that is 1.5 times the interquartile range away from 25th or 75th percentile value.

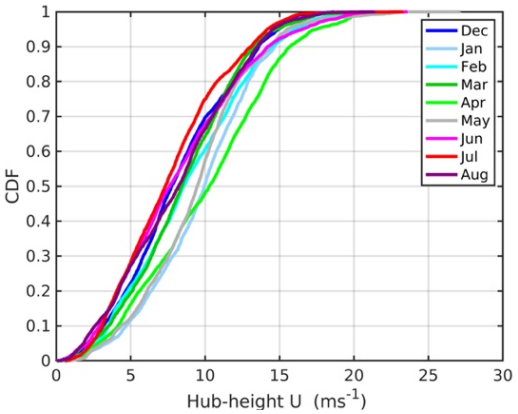

Figure 4. Cumulative probability distribution of 10-minute wind speeds (U) from the noWT domain in the sixth model layer (z = 6) in the centre of the Pomeroy sub-domain in each calendar month.

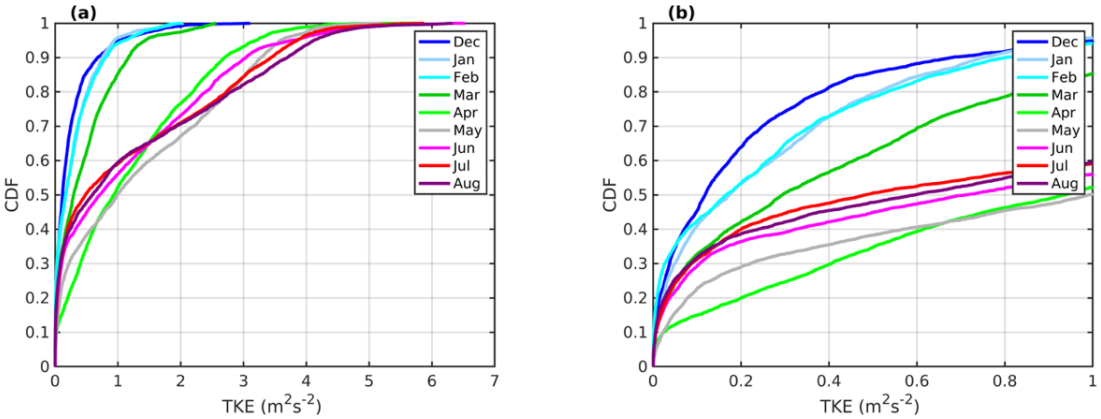

Figure 5. Monthly cumulative probability distribution of 10-minute TKE values at hub-height in the centre of the Pomeroy sub-domain. TKE is from the noWT domain computed by the Mellor-Yamada-Nakanishi-Niino 2.5 PBL scheme. Frame (a) shows the entire CDF, (b) shows only TKE < 1 m^{2}s^{-2}.

4.2 Power production and wake characteristics

In all of the nine simulated months power production in the Pomeroy sub-domain from the EWP scheme

exceeds that from the Fitch scheme (Figure 6). Difference in power output from the two schemes is largest during winter and spring months, when monthly total power production is 5% higher from EWP than Fitch, and smallest during April and May (when the ratio of power production drops to approximately 1.01). The average areal extent of wind farm wake ($v_d \geq 5\%$ i.e. where the velocity deficit exceeds 5% of the freestream wind speed) in the Pomeroy sub-domain as computed using output from Fitch and EWP conditionally sampled by freestream U and TKE in the centre of the sub-domain is shown for March and for data over all nine months in Figure 7. Consistent with *a priori* expectations and results from large eddy simulations of a neutral boundary layer with varying inflow TKE [13], variability in ambient TKE has a profound effect on the spatial extent and intensity of wind farm wakes as simulated using both wind farm parameterizations and specifically on the divergence between the two schemes (Figure 7). Wake extents from both schemes are largest under moderate wind speeds (4–10 ms^{-1}) and low TKE. Under virtually all TKE|U classes the average extent of the wake is larger (i.e. a greater fraction of grid cells have a mean $v_d \geq 5\%$) in simulations with Fitch. This is particularly true for TKE < 0.3 m^2s^{-2} under all wind speeds (Figure 7). Wake extents, as estimated using a 5% fractional velocity deficit, from the two schemes converge as ambient TKE increases (Figure 7).

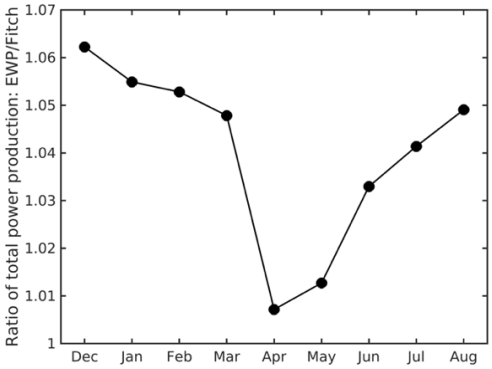

Figure 6. Ratio of monthly total power production from wind turbines in the Pomeroy sub-domain as computed using output from the EWP scheme divided by that from the Fitch wind farm parameterization. Values above 1 indicate higher simulated power production from EWP.

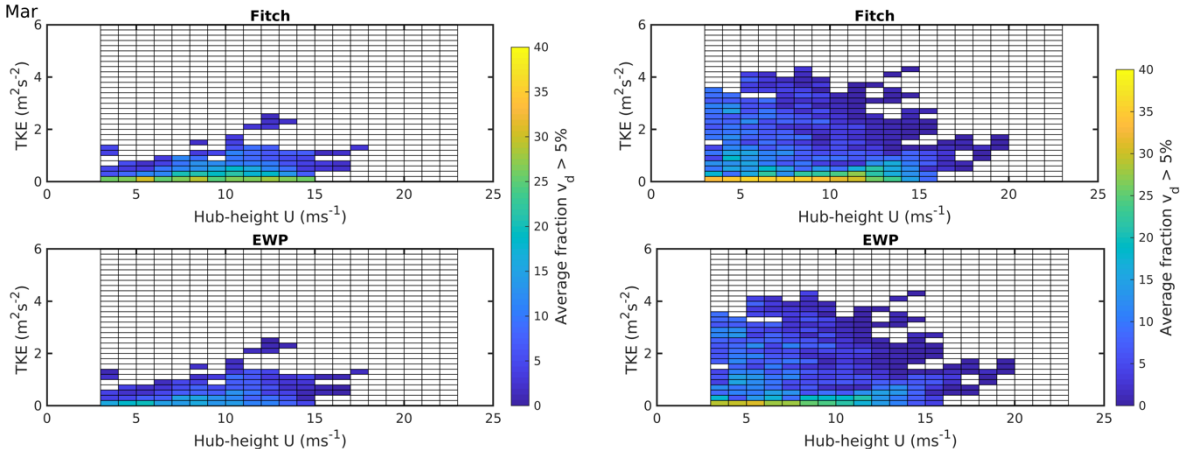

Figure 7. Pseudocolor depictions of the average areal extent of the wind farm wake (i.e. average fraction of the Pomeroy sub-domain where the velocity deficit (v_d) is in excess of 5% of the freestream wind speed) conditionally sampled by the joint probabilities of freestream wind speed (U) and TKE at hub-height from the no-WT domain in a sample month; March (left) and a composite generated using output from all nine months (right). The upper panels show results from Fitch and the lower panels from EWP. Results are only presented in cells (of joint wind speed and TKE) with more than ten members.

Differences in wake extent from Fitch and EWP as a function of U and TKE for all 10-minute periods in the entire 9-month simulation are shown in Figure 8. The values shown in this figure are derived as the average areal extent of wakes in each class of freestream U and TKE from Fitch minus that from EWP (i.e. values from the lower frame in Figure 7 are subtracted from those in the upper panel). There

are very small discrepancies (< 5% difference in the spatial extent of the wake) between the schemes for all wind speeds once TKE exceeds 1 m^2s^{-2}. Although the summer months frequently exhibit freestream TKE values > 1 m^2s^{-2} (Figure 5), a substantial fraction of those are associated with *U* below 4 ms^{-1}, and relatively low TKE dominates at power producing wind speeds (Figure 9). Thus, Figures 10 and 11 present results for analyses confined to freestream TKE < 1 m^2s^{-2}. For TKE < 0.3 m^2s^{-2} and *U* from cut-in to rated, there are very large differences (5-20%) between the areal extent of highly waked ($vd \geq 5\%$) regions simulated by the two wind farm wake parameterizations (Figure 10). There is marked seasonality in the wind farm wake extent and transition towards higher wind speeds and ambient turbulence intensity over the first four months of the year is clearly manifest as a change in the mean spatial extent of fractional velocity deficits of a given magnitude and thus the area influenced by the wind farm wake (Figures 12 and 13). The monthly variation in wind turbine induced TKE is considerably less marked (Figure 12) due to the occurrence of a high frequency of power producing wind speeds in each of these calendar months (Figure 4).

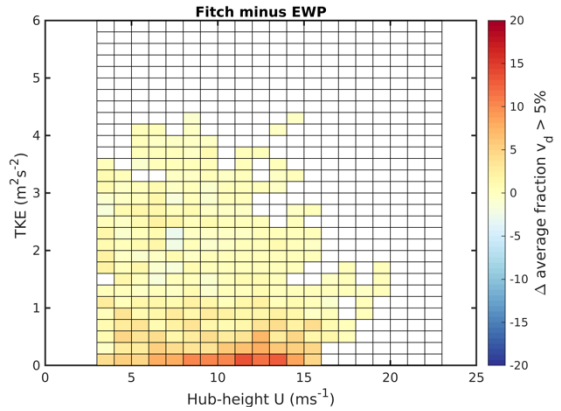

Figure 8. Pseudocolor depiction of the difference in mean areal extent of wakes in the Pomeroy sub-domain (Fitch minus EWP) over the entire 9 months conditionally sampled by the freestream U and TKE. Results are only presented in TKE|U cells with more than ten members.

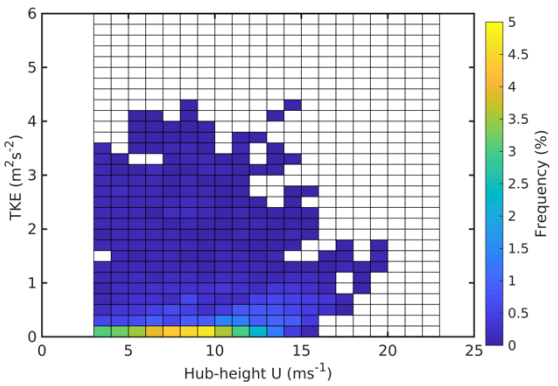

Figure 9. Pseudocolor depiction of the joint probability of freestream wind speed and TKE in different classes over the entire 9-month simulation. Results are only presented in TKE|U cells with more than ten members.

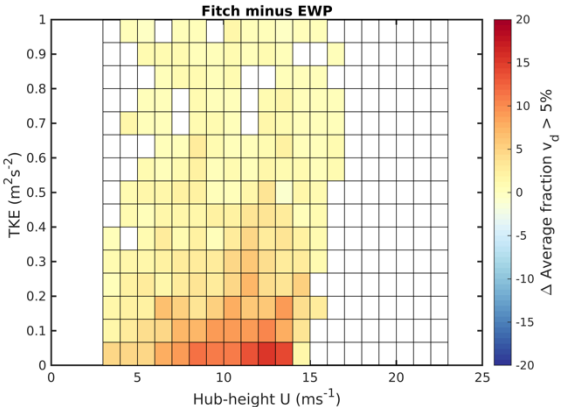

Figure 10. Pseudocolor depiction of the difference in average areal extent of the wind farm wake in the Pomeroy sub-domain (Fitch minus EWP) over the entire 9 months conditionally sampled by the freestream wind speed and TKE.

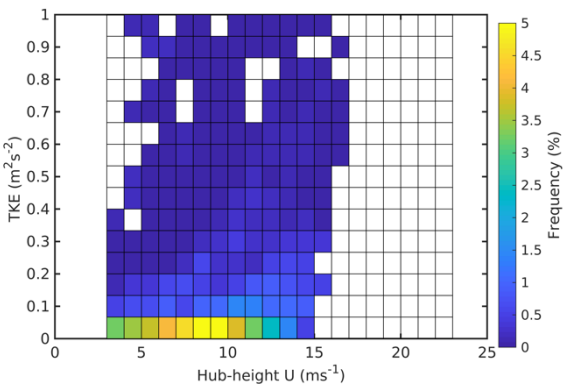

Figure 11. Pseudocolor depiction of the frequency of observations of freestream wind speed and TKE in different classes over the entire 9-month simulation. Values are only shown for TKE = 0 to 1 m^2s^{-2}, and in TKE|U cells with more than ten members.

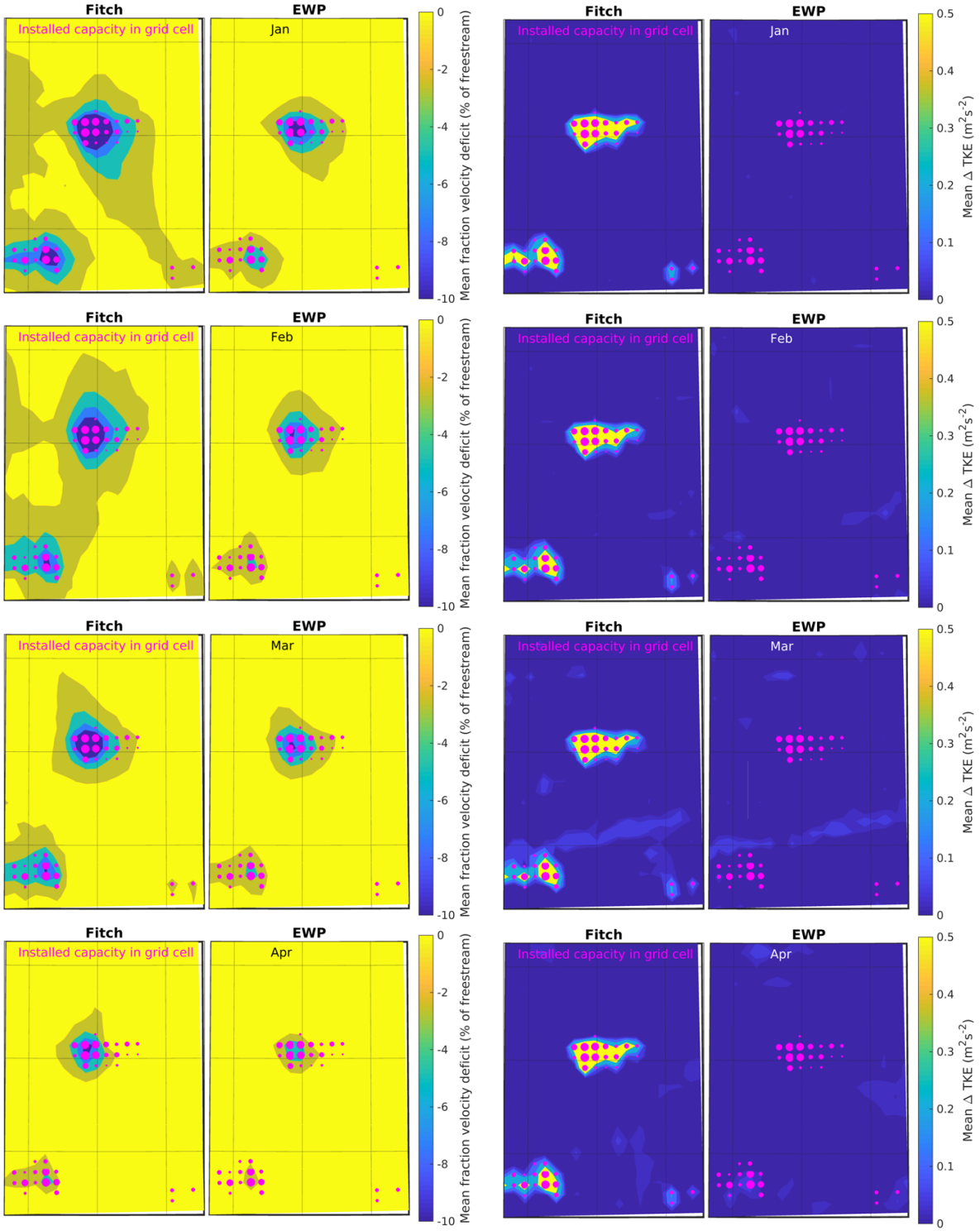

Figure 12. Mean fractional velocity deficit (<$vd_{(x,y)}$>) (left) and TKE perturbation (Delta, right) near WT hub-height (z = 6) relative to the noWT domain from the two wind farm parameterizations (Fitch and EWP) within the Pomeroy sub-domain during the first four calendar months of 2008 (January-April). The <$vd_{(x,y,z,t)}$> values in each grid cell for each 10-minute period in each month are computed as shown in Eq (1) and then averaged over all 10-minute periods in the month. The diameter of the magenta symbols denotes the wind turbine installed capacity within each 4 km by 4 km grid cell.

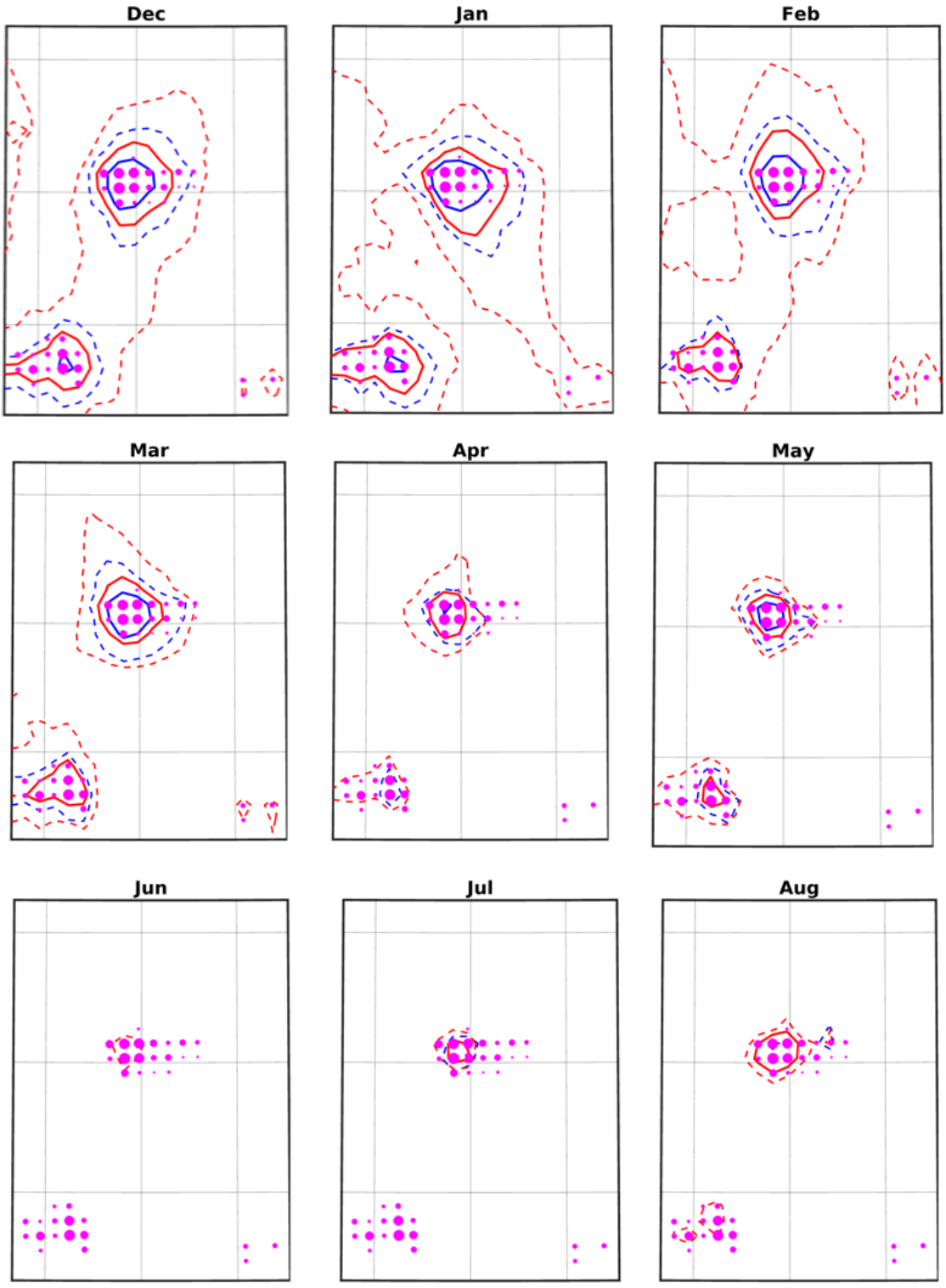

Figure 13. Contours of mean fractional velocity deficits of 5% (solid) and 2% (dashed) from Fitch (red) and EWP (blue) by calendar month (panels) for the Pomeroy sub-domain (see Figure 2). Grid cells containing one or more wind turbine are shown by the magenta symbols. The diameter of the symbols scale with installed capacity within each 4 km by 4 km grid cell.

Areas with mean fractional velocity deficit $<vd_{(x,y)}>$ of > 5% and > 2% are shown for each month from EWP and Fitch in Figure 13. These spatial depictions also exhibit substantial variability by calendar month as a result of the frequency of the occurrence of wind speeds in power producing classes and prevailing freestream TKE. Thus, while wakes tend to be fractionally larger during the lower wind speed months of summer, a lower overall frequency of power producing wind speeds and higher TKE means that wakes are less frequent and less persistent. This is consistent with the above analysis and numerous past studies that have indicated wind turbine wakes are more persistent and spatially extensive in low turbulence conditions offshore [14-16]. Thus the extent of the wake from the Pomeroy cluster (as defined using either a 5% or 2% $<vd_{(x,y)}>$) covers a much larger area in the winter months than during summer (Figure 13). This is true for simulations from both Fitch and EWP but the area covered by $<vd_{(x,y)}>$ > 5% or 2% is consistently larger in output from Fitch, despite explicit addition of TKE in this wind farm parameterization. The implication is that, for the prevailing atmospheric conditions in Iowa, the within grid cell expansion of the wind turbine wake as parameterized in EWP is, on average, more efficient at dissipating wind farm wakes than the addition of TKE as parameterized in Fitch.

The WRF user community has recently identified a possible error within the implementation of the Fitch wind farm parameterization that may be preventing proper advection of wind turbine generated TKE. It is possible that this lack of appropriate TKE advection is leading to artificially enhanced wake lifetimes and thus spatial extents. This effect is illustrated in Figure 12 which shows the enhancement of TKE in the simulation with Fitch is highly localized to grid cells containing wind turbines and appears to be due to an error in the order of operations between TKE advection and modification to the TKE budget from wind turbines. Further investigation of this issue and development of solutions should be the priority for future research. It is worthy of note that experimental data collected downstream of a large onshore wind farm suggest cumulative wind turbine-added turbulence is small relative to the ambient turbulence at a downwind distance from the wind farm edge of 20–30D [17]. For the wind turbines in the Pomeroy cluster this equates to a distance of 1.4 to 3.0 km which is below the grid resolution (of 4 km) used in simulations presented here. Figure 12 also illustrates a key difference in the two wind farm parameterizations. There is little perturbation to TKE in the simulations with EWP because in this wind farm parameterization the wind turbine(s) does/do not act as an active source of TKE. Rather, in EWP the near-wind turbine enhancement of turbulent mixing and wake dissipation is parameterized by the within grid cell expansion of the composite wake and TKE is only impacted via modifications to the wind speed profile.

5. Discussion and Conclusions

Wind farm wake extents in space and conditionally sampled by freestream wind speed and TKE as summarized herein lead to the following key inferences:

- Differences between wake extents and intensities from the two wind farm parameterizations formulated for use with WRF are substantial (Figures 7, 8, 10, 12 and 13). Wind farm wakes (vd > 5%) frequently cover 25% of the Pomeroy sub-domain in simulations with Fitch, but cover considerably smaller areas in simulations with EWP (Figures 12 and 13). For example, at distances of ~ 16 km to the north of the wind farm the mean vd from Fitch is 5% but only 2% from EWP. For mean freestream wind speeds of 8 ms^{-1}, these velocity deficits are 0.4 ms^{-1} (Fitch) and 0.15 ms^{-1} (EWP). These vd would be detectable and differentiable using current lidar technology provided good measurements are also collected regarding the inflow wind speed profile [18, 19].
- Wind farm wake extents are maximized at low TKE (< 0.3 m^2s^{-2}) with U = 4–12 ms^{-1}, and such conditions are relatively frequently observed in Iowa, even during summer months (Figure 8–11). There are also marked differences in wake extents derived from Fitch and EWP under these conditions (Figure 7). Differences between the schemes decrease as the TKE increases (Figure 7 and 8). However, there is a low frequency of high freestream TKE during periods of power-producing wind speeds (Figure 9).

As mentioned above, a partial objective for this research is to illustrate how WRF simulations using wind farm parameterizations might be used to identify where experimental data would be most

beneficial in differentiating relative skill and thus guide optimal instrument siting and experiment timing for a field experiment. Using a fictitious AWAKEN experiment centred on the Pomeroy wind farm cluster, results presented herein provide the following guidance to instrumentation siting and experimental design if the purpose of the experiment is to provide information regarding the relative fidelity of these wind farm parameterizations:

- The experiment should be conducted in low TKE conditions. For the climatology of the U.S. Great Plains it would likely be most beneficial if such an experiment were conducted during the winter season (Figures 5, 12 and 13).
- If the experiment were designed to encompass a full year of data collection it should incorporate a dynamic and seasonally varying equipment deployment strategy to account for the marked seasonality in climate and thus wind farm wake extents. The experimental methodology could involve a simple two-phase design wherein:
    - Stage 1: During the wintertime the instrumentation should be deployed at substantial distances (up to 12 km) from the north and south of the edge of the wind farm
    - Stage 2: During the warm season months the instrumentation should be moved to closer to the edge of the wind farm (Figures 12 and 13).

6. Acknowledgments

This work was supported by the U.S. Department of Energy (DoE) (DE-SC0016438 and DE-SC0016605), and computing resources from the National Science Foundation (ACI-1541215 and TG-ATM170024) and DoE (DE-AC02-05CH11231). The comments of three thoughtful reviewers are acknowledged.

7. References

[1] AWEA, *4th Quarter 2019 Market Report*. 2020, American Wind Energy Association: Available for purchase from http://www.awea.org/. p. 49.

[2] Wind Europe, *Wind Energy in Europe 2018*. 2019, Wind Europe: Brussels. Avialable from: https://windeurope.org/wp-content/uploads/files/about-wind/statistics/WindEurope-Annual-Statistics-2018.pdf. p. 32.

[3] Wind Europe, *Wind Energy in Europe: Outlook to 2023*. 2019, Wind Europe: Brussels. Available from: https://windeurope.org/about-wind/reports/wind-energy-in-europe-outlook-to-2023/. p. 40.

[4] Fitch, A.C., et al., Local and Mesoscale Impacts of Wind Farms as Parameterized in a Mesoscale NWP Model. *Monthly Weather Review*, 2012. **140**(9): 3017-3038.

[5] Volker, P.J.H., et al., The Explicit Wake Parametrisation V1.0: a wind farm parametrisation in the mesoscale model WRF. *Geoscientific Model Development*, 2015. **8**: 3481-3522. https://doi.org/10.5194/gmd-8-3715-2015.

[6] Fitch, A.C., Notes on using the mesoscale wind farm parameterization of Fitch et al.(2012) in WRF. *Wind Energy*, 2016. **19**(9): 1757-1758.

[7] Pryor, S.C., et al., 'Wind theft' from onshore wind turbine arrays: Sensitivity to wind farm parameterization and resolution. *Journal of Applied Meteorology and Climatology*, 2020. **59**: 153-174.

[8] Shepherd, T.J., R.J. Barthelmie, and S.C. Pryor, Sensitivity of wind turbine array downstream effects to the parameterization used in WRF. *Journal of Applied Meteorology and Climatology*, 2020. **59**: 333-361.

[9] Pryor, S.C., et al., Wind farm wakes simulated using WRF. *Journal of Physics: Conference Series*, 2019. **1256**: 012025 doi: 10.1088/1742-6596/1256/1/012025.

[10] Pryor, S.C., R.J. Barthelmie, and T. Shepherd, The influence of real-world wind turbine deployments on regional climate. *Journal of Geophysical Research: Atmospheres*, 2018. **123**: 5804-5826.

[11] Pryor, S.C., R.J. Barthelme, and T. Shepherd, 20% of US electricity from wind will have limited impacts on system efficiency and regional climate. *Scientific Reports*, 2020. **10**: doi: 10.1038/s41598-019-57371-1.
[12] Freire, L.S., et al., Critical flux Richardson number for Kolmogorov turbulence enabled by TKE transport. *Quarterly Journal of the Royal Meteorological Society*, 2019. **145**(721): 1551-1558.
[13] Wu, Y.-T. and F. Porté-Agel, Atmospheric turbulence effects on wind-turbine wakes: An LES study. *Energies*, 2012. **5**(12): 5340-5362.
[14] Christiansen, M.B. and C.B. Hasager, Using airborne and satellite SAR for wake mapping offshore. *Wind Energy*, 2006. **9**(5): 437-455.
[15] Barthelmie, R.J., K.S. Hansen, and S.C. Pryor, Meteorological controls on wind turbine wakes. *Proceedings of the IEEE*, 2013. **101(4)**: 1010-1019.
[16] Volker, P.J.H., et al., Prospects for generating electricity by large onshore and offshore wind farms. *Environmental Research Letters*, 2017. **12**(3): 034022.
[17] Smith, C.M., R.J. Barthelmie, and S.C. Pryor, In situ observations of the influence of a large onshore wind farm on near-surface temperature, turbulence intensity and wind speed profiles *Environmental Research Letters*, 2013. **8**: 034006.
[18] Fernando, H.J.S., et al., The Perdigão: Peering into Microscale Details of Mountain Winds. *Bulletin of the American Meteorological Society*, 2018. **100**: 799-819.
[19] Barthelmie, R.J. and S.C. Pryor, Automated Wind Turbine Wake Characterization in Complex Terrain. *Atmospheric Measurement Techniques*, 2019. **12**: 3463-3484.